Astron. Astrophys. 298, 505–516 (1995)

ASTRONOMY AND ASTROPHYSICS

The discovery of a very active high proper motion dMe binary star*

G. Micela[1], F. Favata[2], J. Pye[3], and S. Sciortino[1]

[1] Istituto e Osservatorio Astronomico di Palermo, Palazzo dei Normanni, I-90134 Palermo, Italy
[2] Astrophysical Division - ESA/ESTEC Postbus 299, NL-2200 AG Noordwijk, The Netherlands
[3] Department of Physics and Astronomy, University of Leicester, Leicester, LE1 7RH, UK

Received 5 July 1994 / Accepted 30 October 1994

Abstract. We present X-ray and optical observations of G102-21, a newly discovered dMe flare star in the solar neighborhood. The star, which falls serendipitously in a pointed PSPC ROSAT observation, shows an intense X-ray flare as well as other, lower-amplitude variations on time scales of around 10^4 seconds. The decay time of about 1000 sec, the characteristics of its X-ray spectrum, and the derived physical parameters, make the observed flare similar to compact solar flares and to many other flares observed on dMe stars, by previous missions.

Low resolution spectroscopic observations show the whole Balmer series and the CaII H&K lines strongly in emission. Monitoring of the equivalent width of the Hα, Hβ and CaII H&K lines shows sizable night to night variations, with flaring-like behavior. Both $H\alpha$ and $H\beta$ lines show the presence of two components, which are very clearly separated at high resolution. The relative radial velocity changes from night to night, indicating a binary system. Based on simple assumptions we estimate that the system has a period of less than 1 day. The rotational broadening of the photospheric absorption lines observable in the high resolution spectra allows us to measure the stellar rotational velocity. The observed value (about 20 km/s) is compatible with a tidally-locked system with a period between 0.5 and 1 day. The X-ray observations are consistent with a period in the range of 14–15 hours and with an inclination of the rotation axis near 50°.

Key words: stars: activity – stars: G 102-21 – stars: close binaries – stars: coronae – stars: flare – X-rays: stars

1. Introduction

X-ray emission from stellar coronae covers a wide range in luminosity (Vaiana et al. 1981); early dM stars in particular have luminosities ranging from 10^{26} to 10^{29} erg sec^{-1}, with nearby younger stars having a mean X-ray emission level higher than that of old stars (Barbera et al. 1993).

Systematic investigations of time variability of coronal emission from dM and dMe stars have been performed both with data taken with the *Einstein* (Giacconi et al. 1979) and the EXOSAT (White & Peacock 1988) observatories. Ambruster et al. (1987) have shown that short-time variability (from several minutes to hours), with typical amplitude of 30-50% is a common phenomenon in M stars seen with *Einstein*. The continuous time coverage of EXOSAT allowed confirmation of the presence of flaring activity from these stars, superimposed on quiescent emission which itself is highly variable (Pallavicini et al. 1990). The characteristics of the observed variability suggest that it is due to magnetic processes, similar to those present in the Sun, including both flares and gradual variations associated with the emergence of magnetic flux in individual active regions. However, the qualitative similarity with the solar case does not correspond to a quantitive one, in the sense that the observed variations associated with the stellar quiescent emission are at most of a factor 2-3 (Pallavicini 1993), much weaker than those observed in the emission level of the Sun,which varies by more than a factor 10 (Vaiana & Rosner 1978). It is worthwhile to note however that the level of X-ray emission of the Sun is about two orders of magnitude lower than that of the brightest dM stars on which variability studies have been feasible, hence an enhancement in X-ray emission by a factor ten on the Sun would correspond, in absolute terms, to only a 10% variation in the most active stars.

Serendipitous X-ray and EUV observations have allowed the detection of peculiar objects and have shown the existence of populations of stars with high activity levels, under-represented in the solar neighborhood (see for example Smale et al. 1986; Favata et al. 1988; Fleming et al. 1989; Jeffries & Bromage 1993; Sciortino et al. 1995).

In this paper we present data on the X-ray observation and follow-up optical observations of the very active dM3 star G102-21, serendipitously detected in the course of a ROSAT (ROntgenSATellit; Trumper 1990) Position Sensitive Proportional Counter (PSPC; Pfeffermann et al. 1986) observation pointed on the star Gl 213. G102-21 is a high proper motion

Send offprint requests to: G. Micela

* Based on observations collected at the DAO Victoria and ESO La Silla observatories

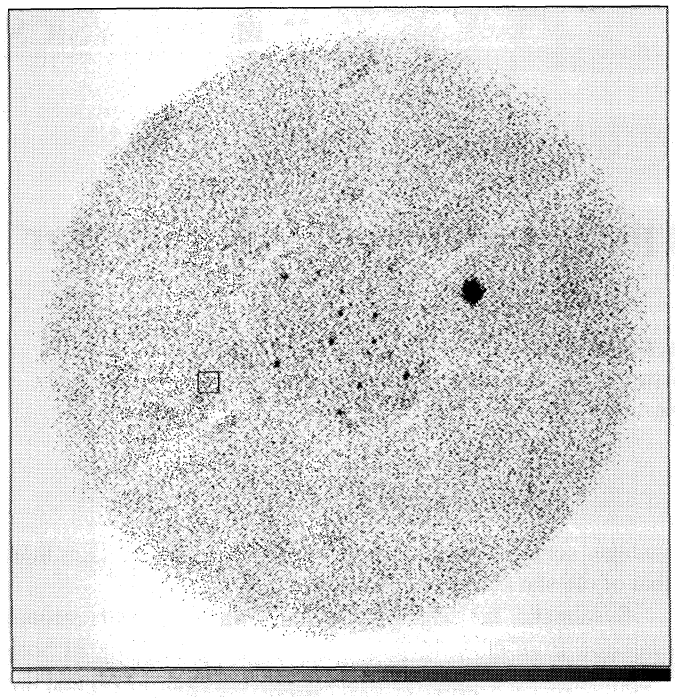

Fig. 1. ROSAT PSPC X-ray image pointed on the star Gl 213. North is up and east is to the left. The strong source at $\sim 30'$ off-axis angle and west of field center is G102-21. The region we have used to evaluate the background is indicated by a square box (towards the east side of the image)

(μ_{ra} = -0.039±0.008 sec and μ_{dec} =-0.277±0.021") star listed in the survey of Giclas et al. (1963); its spectral type has been determined by Lee (1984). Its characteristics are very similar to those of the star Gl 841A, an active short-period binary system discovered by Jeffries & Bromage (1993) during the ROSAT Wide Field Camera (WFC; Sims et al. 1990; Pounds et al. 1993) EUV all-sky survey. The G102-21 magnitude reported in the CNS3 catalog (Gliese & Jahreiss 1991) is m_v=11.36; assuming an absolute magnitude M_V = 10.4 (Lang 1980), we obtain a distance of 15.6 pc.

2. X-ray data

X-ray data were collected with the ROSAT PSPC between 21 and 25 September 1993, yielding a total useful exposure time of $\sim$ 14 ksec. The image shown in Fig. 1 reveals the presence of a strong source at an off-axis angle of $\sim 30'$, on the external side of the central circular part of the PSPC entrance window support structure. The Standard Analysis Software System (SASS) confirmed, at this position, a source with a mean count-rate of ~ 0.5 counts sec^{-1}, and identified with the high proper motion star G102-21. No other object listed in the SIMBAD database is present in a box of 240" centered on the X-ray centroid position.

The light curve of this source as determined by SASS shows an intense flare and other variations of smaller amplitude.

We have not found other published X-ray observations of this star, but a search in the stellar X-ray *Einstein* database (Sciortino et al. 1988; Harnden et al. 1990) reveals that G102-21 has been observed and detected serendipitously (at $\sim 27'$ off-axis angle) with the *Einstein* Imaging Proportional Counter (IPC) in the observation sequence number I3108, performed on 27 March 1979. Its *Einstein* IPC (0.16-3.5 keV) rate measured in a 3' radius circle was 0.095 cnt/sec. Adopting the standard conversion factor 2 10^{-11}erg cm^{-2} typical of unabsorbed coronal sources (Vaiana et al. 1981), we obtain a flux of 1.9 10^{-12}erg sec^{-1} cm^{-2}, and a luminosity L_X = 5.5 10^{28}erg sec^{-1}. The short observation time ($\leq$ 2000 sec) prevents us any detailed spectral or time analysis on *Einstein* data.

2.1. Data analysis

The X-ray source falls outside the central part of the field of view and near one of the radial supports of the PSPC entrance window. Given its field–of–view position and the telescope wobble, temporally resolved data analysis, such as that we intend to pursue, requires great care in order to treat properly the effects of possible partial shadowing of the source, by the PSPC entrance window support structure.

In the following, we have performed our analysis in the energy band 0.20-2.02 keV, corresponding to the PSPC Pulse-height Independent (PI) channels from 20 to 201. We have chosen this energy band because at lower energy the instrument suffers from the so-called electronic ghost image problem, and at higher energy the instrument map, necessary for computing the exposure map, is not available.

In Fig. 2 we show the spatial distribution of counts around the X-ray source position. The cross marks the position of the source centroid at R.A. (2000) = $5^h40^m16^s.4$ and Dec. (2000) = $12°39'13".7$. This figure clearly shows the asymmetry and the "hole" in the Point Response Function (PRF) at this large off-axis angle. The square region 4' on a side, shown as a box in Fig. 2, has been used to compute mean exposure time and source rate, while for the spectral analysis we have retained all counts inside the 2.8' radius circle[1] shown in Fig. 2.

To determine the effective exposure time at the source position we have computed exposure maps adopting the procedure[2], based on the results of the analysis of the ROSAT PSPC all sky survey data by Snowden et al. (1994), that takes into account vignetting, entrance window non-uniformities, support structure and wire shadowing, telescope wobble and other variations of pointing direction with time. We have adopted as template an instrument map in the 0.20-2.02 keV band obtained by sum-

[1] Note that $\sim$ 95% of the counts fall in a 2' radius circle

[2] This procedure is coded in the "make_emap" algorithm, we have used, distributed by the High Energy Astrophysics Science Archive Research Center (HEASARC) at Goddard with ROSATLIB (Reichert 1993), a collection of procedures for use within the Interactive Data Language (IDL, a registered trademark of Research Systems, Inc.)

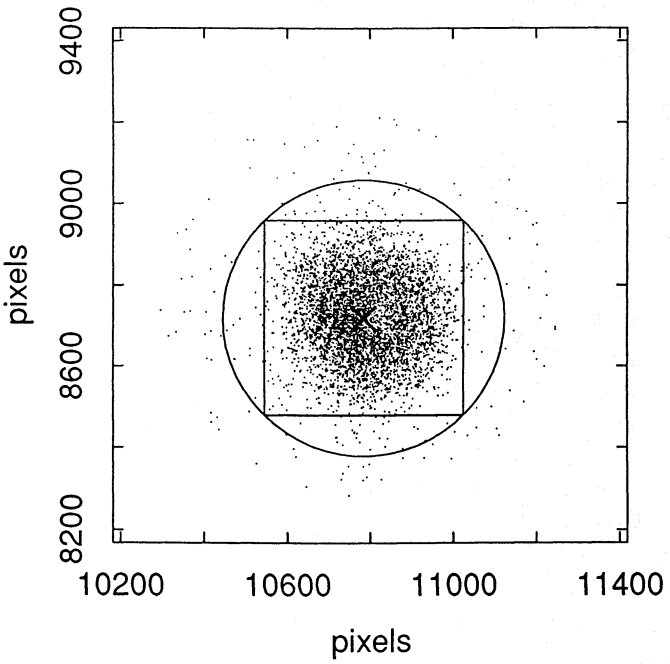

Fig. 2. Spatial distribution of X-ray photons around the source centroid (indicated with a cross). The coordinates are in instrumental pixel units (1 pixel = 0.5 arcsec). The square indicates the region we have used to evaluate the source rates, while the circle is the region we have used to extract photons for spectral analysis purposes

ming up the six available instrument maps (Snowden et al. 1994) weighted according to the overall image spectrum.[3]

Source rates have been computed by dividing source counts collected in the $4' \times 4'$ box by the mean value of the exposure map over the same region. We have repeated this procedure for three distinct energy bands, namely: broad (PI channels 20-201), soft (PI channels 20-69), and hard (PI channels 70-201). The derived exposure times are 10864 sec (to be compared with an on-axis on-time of 14026 sec), 11159 sec, and 10469 sec, respectively (the difference in exposure times, of the order of 3%, is due to the energy dependence of the instrument maps). The numbers of counts collected in the broad, soft and hard bands are 5807, 3069 and 2738, respectively. The deduced rates are 0.535 ($\pm$1.3%), 0.275 ($\pm$1.8%) and 0.262 ($\pm$1.9%) in the broad, soft, and hard bands, respectively; quoted errors are due to counting statistics. The broad-band background rate, evaluated as indicated in Fig. 1, integrating counts over an area equal to that of the source collection region at the opposite side of the field of view, is about 8.5 10^{-3} cnt/sec. It accounts for 1-2% of the source rate and is comparable with its statistical uncertainty. In the analysis of the light curve we ignore the background contribution and consider all collected counts as due to the source.

[3] This summing procedure is suggested in the ROSAT Extended Scientific Analysis System (EXSAS) User's manual (Zimmermann et al. 1993).

2.2. *Light curve and spectra*

The source light curve shows that the emission is highly variable. The entire observation, spanning 3.35 days, is subdivided in 8 different time segments, with on-times in the 0.7-2 ksec range. For each of these time segments we have separately evaluated the count rates with the same procedure adopted for the entire observation. In Table 1 we summarize the data for each individual time segment in the broad, soft and hard bands. An inspection of Table 1 shows that, in the broad band, the coronal emission of G102-21 has varied up to a factor 7 with respect to its minimum (quiescent?) level; the observed variation increases up to a factor $\sim$ 10 in the hard band.

The hardness ratios (defined as the ratio of the hard and soft rates) show no statistically significant variation during the entire observation, with the exception of segment 5 where both the intensity and the hardness ratio achieve their maximum values.

In order to study the nature of the observed variability, we have evaluated the source light curve at a 200-second bin size. For *each individual* time bin we have computed the exposure map, and have evaluated the source rate from collected source counts and exposure time at the source position. This step is necessary because the ratio between the effective live time and the on-time is not constant, as would be expected for an ideal detector without wobble and/or without the entrance window support structure, but at the specific source position and for this observation this ratio ranges between 0.57 and 0.85. The resulting light curve is shown in Fig. 3, where times are measured from the beginning of the observation, namely UT 22:09:48 September 21st 1991. It is noteworthy that we cannot adopt a smaller bin size, because the temporal resolution and the intrinsic uncertainties of the satellite aspect information limit, for temporal resolution lower than 200 sec, the proper removal of intensity modulations due to the telescope wobble. In particular we have verified that for time bins of 100 seconds, strong residual effects of telescope wobble are clearly visible in the deduced source rates.

To better assess source spectral variations we have separately fitted the spectra collected in each of the 8 segments with 1-temperature and 2-temperature Raymond-Smith (Raymond & Smith 1977; Raymond 1988) models, using the fitting algorithm implemented in the Post-Reduction Off-line Software (PROS) V2.2.3 developed by the High Energy Astrophysical Division of the Smithsonian Astrophysical Observatory. In the fitting procedure we have included a 2% systematic error required (cf. Fiore et al. 1994) to allow for residual uncertainties in the "January 1993" PSPC response matrix. Given the source distance, the effect of interstellar absorption on X-ray emission is negligible, and for fitting X-ray spectra we have assumed $\log N_H = 18$. Because of the telescope wobble and the entrance window support structure, we have not been able to find an ideal region for computing the background, i.e. a region unaffected by the support-structure shadowing and having the same exposure time as the region where the source counts have been collected. However, we have verified that the exposure times in the eights segments, evaluated in the "background" square region of Fig. 1 differ from those evaluated in the source region by only 7% to

Table 1. Summary of data in each time segment

Time Segment	1	2	3	4	5	6	7	8
Start Time* [sec]	0	1595	5739	109835	139230	144870	281849	287803
Ontime [sec]	1593	1431	2956	2107	731	995	2202	1979
			SOFT BAND					
COLLECTED COUNTS	250	190	945	246	444	109	520	360
EXPOSURE TIME	1261	1128	2327	1743	601	776	1721	1560
SOURCE RATE†	0.20	0.17	0.41	0.14	0.74	0.14	0.30	0.23
RATE ERROR	0.01	0.01	0.01	0.01	0.04	0.01	0.01	0.01
			HARD BAND					
COLLECTED COUNTS	205	167	833	188	576	82	365	321
EXPOSURE TIME	1183	1059	2181	1639	564	729	1613	1462
SOURCE RATE†	0.17	0.16	0.38	0.11	1.02	0.11	0.23	0.22
RATE ERROR	0.01	0.01	0.01	0.01	0.04	0.01	0.01	0.01
			BROAD BAND					
COLLECTED COUNTS	455	357	1778	434	1020	191	885	681
EXPOSURE TIME	1227	1099	2264	1698	585	756	1675	1518
SOURCE RATE†	0.37	0.32	0.79	0.26	1.74	0.25	0.53	0.45
RATE ERROR	0.02	0.02	0.02	0.01	0.05	0.02	0.02	0.02
HARD/SOFT	0.87	0.94	0.94	0.81	1.38	0.80	0.75	0.95
ERROR	0.12	0.14	0.31	0.11	0.12	0.17	0.07	0.10

*Time is counted from the beginning of the observation

†As discussed in the text, background contribution is negligible

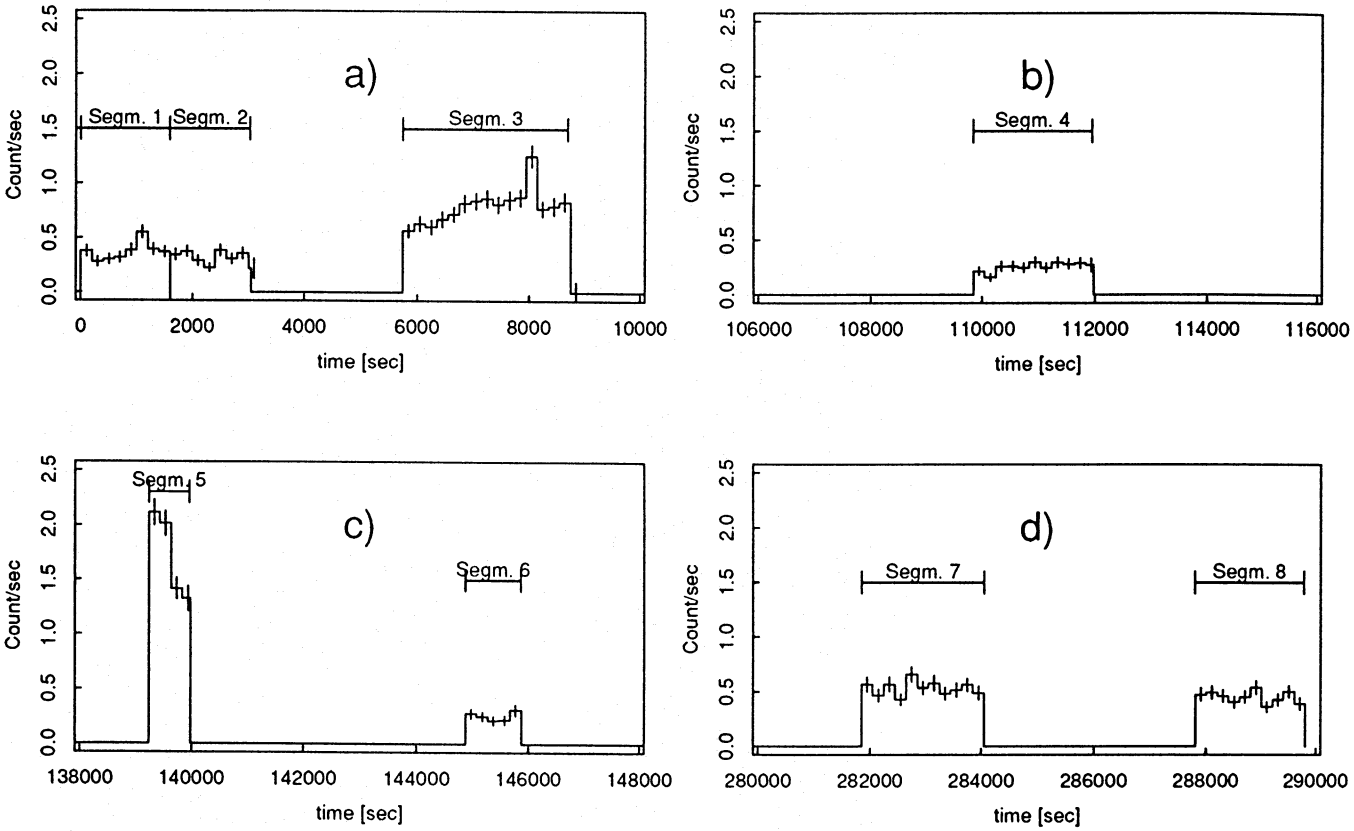

Fig. 3. Light curve of the X-ray source binned in intervals of 200 sec, corrected for the wobble and variations in the exposure as described in the text

21%. In order not to introduce further sources of uncertainty we have not attempted background subtraction, after having verified that the inclusion of its small contribution does not modify significantly the results of the spectral fits.

Results of the 1-temperature model fitting are summarized in Table 2 together with the number of source counts[4]. The fits have been extended to the energy range 0.2-2.4 keV corresponding to the PI channels 6-34 (in the 34 re-binning scheme adopted in the PROS fitting algorithm). In the case of the 1-temperature model, two parameters: temperature and associated emission measure, are estimated by the least-squares fitting procedure, yielding a χ^2 with 27 degrees of freedom. In the case of the 2-temperature model, four parameters: low and high temperature, the ratio of their emission measures and the value of the emission measure for the low temperature component, are estimated by the fit procedure yielding a χ^2 with 25 degrees of freedom. The single temperature fit does not furnish a statistically adequate (at the 95% confidence level) description of the observed emission for most of the observation, namely in segments 1, 3, 4, 7 and 8. In two cases (segments 2 and 6) the value of χ^2 obtained with the 1-T fit does give an acceptable value, but, at least in segment 2 where the statistics allow us a similar study, the residuals, shown together with the fitted spectrum in Fig. 4, show systematically positive values at the softest energies and negative above 1 keV. This indicates that the fitted model does not furnish an adequate description to the data. Hence we have performed 2-T fits in this latter case also. Again in segment 6 the residuals seem to have the same systematic behavior, but the low statistics prevent us from performing any spectral fit with more parameters. In segment 5 (the segment showing the flare) the 1-T fit is acceptable too. In this case the 2-T fit confirms the hard nature of the spectrum, resulting in an emission measure of the high temperature component about one order of magnitude larger than the emission measure of the cool component. In the remaining cases a second temperature is required for an acceptable fit.

As extensively discussed by Maggio et al. (1994a,b) a PSPC spectrum with about 150 counts can constrain the temperature of a single-temperature Raymond-Smith model when this is lower than ~ 0.3 keV, while its value is substantially less constrained for kT ≥ 0.5 keV. When the number of counts increases up to 300, the fit of a two-temperature Raymond-Smith model gives a constrained low temperature (for kT ~ 0.2 keV) and constrained high temperature (for kT ~ 1 keV) when the ratio $EM_{high}/EM_{low} \gtrsim 1$. They have also shown that with these count statistics a double temperature spectrum cannot be adequately described by a single temperature fit. Since in all the considered time segments (with only the exception of segment 6) the number of collected counts is greater than 380 counts, there is no doubt of the need to include, when required, (at least) a second thermal component.

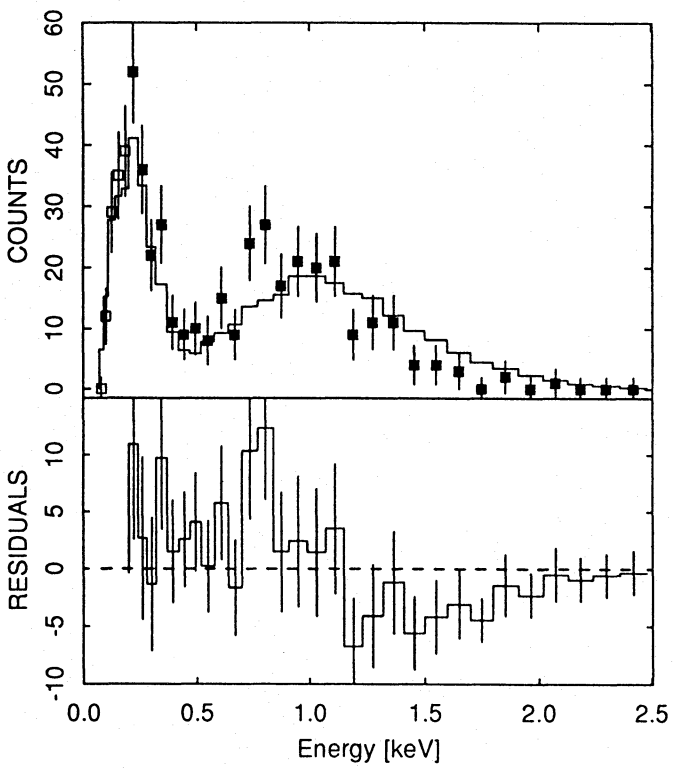

Fig. 4. Fitted (solid line) and observed (squares) spectra for segment 2. Filled symbols indicate channels used in the fit. The residuals (observed – expected) show a systematic trend, positive at the softest energies and negative above 1 keV

In Table 2 we report also the source flux at earth, in the 0.20-2.02 keV energy band, and the X-ray luminosity obtained in each of the eight time segments, assuming a distance of 15.6 pc. The X-ray luminosity ranges between $\sim 7\ 10^{28}$ erg sec^{-1} and $5\ 10^{29}$ erg sec^{-1}, with the maximum value being reached during the flare.

In the quiescent segments (1, 2, 4, and 6) the star does not significantly vary its emission level, with L_X values discrepant at most by 50%. In segments 7 and 8 the emission goes up by a factor 2 above the minimum, while in segment 3 the emission is four times higher than the quiescent level. During the "flare" (segment 5) the emission is $\sim 7 - 8$ times more intense than in the quiescent phase. Even if we consider the quiescent emission level, G102-21 with a value of $L_X \sim 7\ 10^{28}$ erg/sec certainly belongs to the high X-ray luminosity tail of the young, early M nearby stars (Barbera et al. 1993). We note that the quiescent emission level determined with the ROSAT data is very similar to that obtained with the *Einstein* IPC 14 years earlier.

To explore the uncertainties in fitted parameters we have performed a grid of spectral fits for each segment[5]. In particular we have computed a three-dimensional grid using as interesting

[4] The numbers of counts are slightly higher that those reported in Table 1 because of the different collection area adopted for extracting source spectra.

[5] We have used the *search_grid* task available in PROS that computes the best fit to a spectrum over a two-dimensional grid of so-called interesting parameters and minimizes with respect to the remaining parameters.

Table 2. Spectral parameters for each time segment

Time Segment	1	2	3	4	5	6	7	8
Source Counts	467	374	1840	454	1045	199	921	699
Single Temperature Model								
T [keV]	2.70	2.68	3.43	3.09	1.18	3.89	2.93	2.14
log EM [cm^{-3}]	52.09	52.04	52.46	51.92	52.60	51.98	52.26	52.24
$\chi^2(27dof)$	40.18	32.19	55.85	59.06	28.08	21.07	96.06	52.25
Probability	0.951	0.775	0.999	1.000	0.593	0.217	1.000	1.000
f_X [10^{-12}erg $cm^{-2}s^{-1}$]	4.05	3.62	9.18	2.69	19.0	2.76	5.71	4.91
L_X [10^{28} erg/sec]	11.8	10.5	26.7	7.85	55.4	8.05	16.6	14.3
Double Temperature Model								
log EM_1 [cm^{-3}]	51.24	51.24	51.42	51.08	51.65	...	51.47	51.16
T_1 [keV]	0.17	0.21	0.20	0.15	0.41	...	0.18	0.15
log EM_2/EM_1	0.27	0.30	0.77	0.15	0.89	...	0.25	0.60
T_2 [keV]	0.92	1.04	1.42	0.80	1.37	...	1.01	1.05
$\chi^2(25dof)$	9.26	11.44	26.43	11.85	10.94	...	16.01	22.82
Probability	0.002	0.009	0.615	0.012	0.007	...	0.085	0.412
f_X [10^{-12}erg $cm^{-2}s^{-1}$]	3.62	3.46	8.72	2.41	19.4	...	5.51	4.40
L_X [10^{28} erg/sec]	10.5	10.1	25.4	7.02	56.6	...	16.0	12.8

parameters the two temperatures and the ratio of the two emission measures, and minimizing with respect to the emission measure of the cool component. The extension of the interesting parameter volumes inside the surfaces corresponding to the minimum χ^2 plus 3.50, 6.25, and 11.30 gives an estimate of uncertainties of those parameters at 68%, 90%, and 99% confidence levels, respectively (Avni 1976). Figs. 5a, 5b and 5c show the allowed ranges of derived temperatures and of the ratio of the two emission measures for each data segment.

2.2.1. The cool component

As shown in Fig. 5a the temperature of the cool component is the same in each segment, regardless of the intensity of the emission. Results for segment 6 are not presented since the available data do not warrant a two-temperature fit. Only during the flare (segment 5) does the low temperature tend to be higher than in the other segments, but this apparent increase of temperature is marginal and we cannot reject the hypothesis that during the flare the low temperature has the same value as the rest of the observation. The emission measure of the low temperature component during the flare is increased by about a factor 2 with respect to the value 2 10^{51} cm^{-3}, typical of all other time segments with the possible exception of segment 7 which shows a slightly larger value.

2.2.2. The hot component

In Fig. 5b we show the allowed ranges for the high-temperature value; this is less constrained since the ROSAT mirrors drastically limit the sensitivity to photons with energy higher than ~ 2 keV, preventing a better determination of the high-temperature value. However, the spectral fits require the presence of a hot component having a temperature greater than ~ 1 keV, whose emission measure, as shown in Fig. 5c, is larger than that of the low temperature component.

In contrast to the cool component, the emission measure of the hot component changes with time. The high temperature component is responsible for the variation of emission level in segments 3 and 5, where the high temperature emission measure is about ten times larger than the low temperature emission measure, while this ratio is less than two during the quiescent phase and about four in segment 8.

2.3. The flare

The light curve shows the occurrence of an intense X-ray flare whose (unseen) maximum occurs before 139 ksec from the beginning of the observation. The observational gaps do not allow us to observe the rising phase of the flare, preventing the determination of the flare maximum. We can only state that the maximum of the emission in the broad band is $\gtrsim 2$ cnt/sec. Assuming a quiescent level of 0.25 cnt/sec the flare increases the star's X-ray emission by at least a factor 7-8.

The shortness of time segment 5 does not allow us to follow in detail the flare decay phase. On the basis of available data we can only derive a rough estimate of decay time, $\tau \sim 1000$ sec. The peak of the X-ray luminosity is $L_X \gtrsim 5.7\ 10^{29}$ erg/sec, with a flare released energy in the (0.2-2.02) keV X-ray band of $E \gtrsim 5\ 10^{32}$ erg.

To estimate the order of magnitude of the physical parameters of the coronal structure in which the flare originated, we have used the scaling law of Reale et al. (1993), obtained for a compact flare, linking the decay time, τ_L, with the semi-length

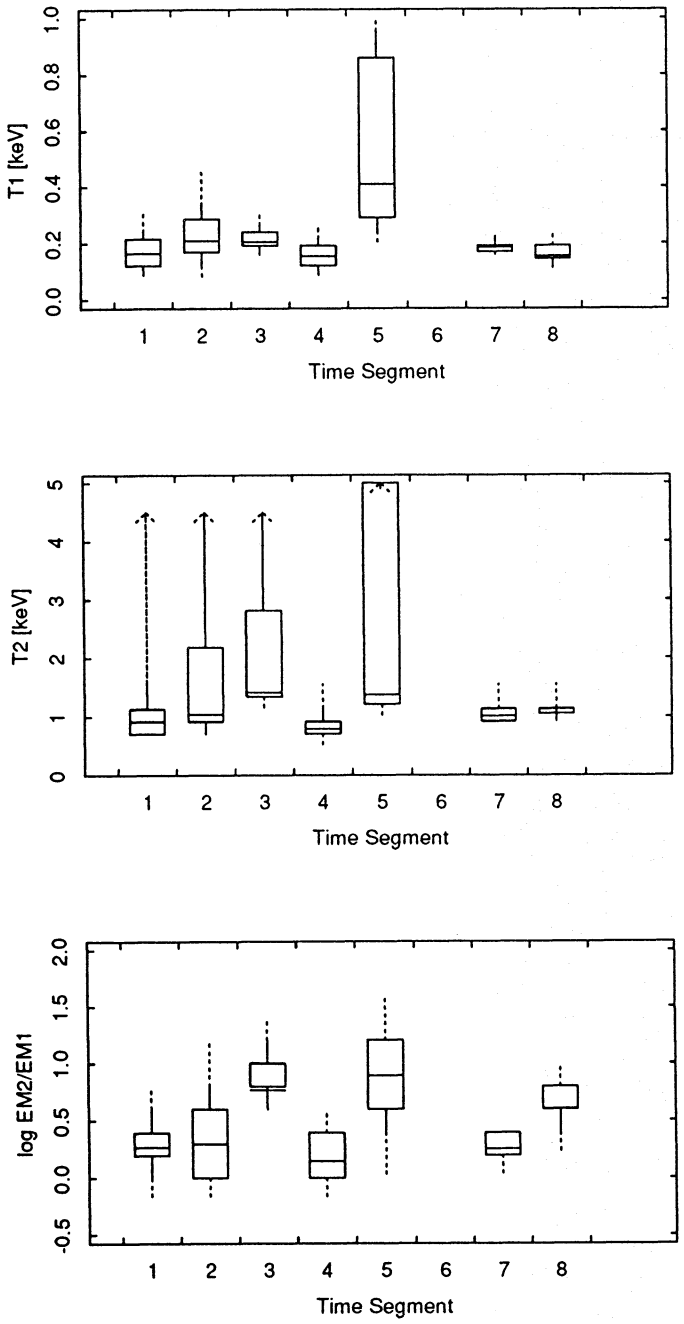

Fig. 5. Range of allowed low (panel a), high (panel b) temperature and of the ratio of the two emission measures (panel c) in the eight time segments. Results for segment 6 are not presented since the 1-T fit results together with low statistics does not warrant to perform a two temperature fit. The range defined by the box corresponds to 68% confidence level, while the ranges identified by the solid and dotted lines indicate the permitted values at 90% and 99% confidence levels, respectively. The arrows indicate values not constrained by the fit

of a single loop L and the temperature T at the top of the loop, assuming the flare heating is abruptly switched off (exponential decay time of the heating term $\tau_H = 0$)

$$\tau_L = \frac{3.7\ 10^{-4}}{\sqrt{T}} \cdot L\ e^{0.5L/H_p} \quad (1)$$

where $H_p = 2kT/g\mu$ is the initial pressure scale height, i.e. the value of the pressure scale height computed just before the decay phase of the flare (Reale et al. 1993).

Using a value of $\tau_L = 1000$ sec and $T = 1.3[-0.2, +0.9]10^7$ K (obtained from the 1-Temperature fit where uncertainties in square brackets are computed at the 99% confidence level), and assuming a gravity twice that of the Sun, appropriate for a dM3 star, we obtain a gravitational scale height of 3 $[-0.3, +2.5]$ 10^{10}cm and a semi-length of the loop of 8.5 $[-0.5, +3.5]$ 10^9cm. This value decreases if the heating function evolves with an exponential decay time ($\tau_H > 0$, Reale et al. 1993)

The 1-T fit gives an emission measure of 4 10^{52} cm^{-3}; assuming a loop of constant section with radius of the order of one tenth of the length of the loop we obtain an estimate of particle density, n_L:

$$n_L \geq \left(\frac{E_m}{L^3 10^{-2}\pi}\right)^{1/2} \sim 1.4[-0.7, +0.4]\ 10^{12}\text{cm}^{-3} \quad (2)$$

where the equality holds if $\tau_H = 0$.

The parameters of this flare are very similar to many of those observed with EXOSAT on other dMe stars (Pallavicini et al. 1990). The time scale is similar to those observed in compact solar flares (Pallavicini et al. 1977), where the spatial structure of the magnetic field remains substantially unchanged during the flare. We note, however, that the flare on G102-21 (like those observed in many other dMe stars) has a larger emission measure, implying a larger volume and density than those observed in compact solar flares.

From the parameters determined above we can perform a rough estimate of the magnetic field needed to confine such a loop by imposing the condition that the magnetic pressure is higher than gas pressure, namely:

$$\frac{B_L^2}{8\pi} \gtrsim 2\pi n_L KT \quad (3)$$

obtaining $B_L \gtrsim 630[-180, +350]$ Gauss, similar to the magnetic fields derived for the stellar flares in dM stars observed by EXOSAT (Pallavicini et al. 1990).

A final note of caveat on the above derived quantities is in order. They have been derived under the assumption that the flare occurs in a single loop. If the event we see in X-rays is instead due to the superposition of several flares occurring at the same time on an arcade of N loops, the derived estimates will change accordingly. In this case the relevant quantity is the total cross-section of the ensemble of flaring loops. If we assume that all the loops have the same radius/length ratio of one tenth assumed before, then the particle density (in each loop), n_l, cannot be lower than $n_L/\sqrt{N}$, and the intensity of magnetic field would

scale as $B_l \sim B_L/N^{1/4}$. On the other hand, if the X-ray event we have seen were instead due to the superposition of several flares starting at different times and with variable durations, then the above analysis cannot be applied. We note however that, since the observed decay time is similar to that of compact solar flares, we have assumed that the observed flare occurred in one (or at most few) loop(s) whose magnetic configuration should not have been substantially changed by the flare itself. Hence we have not attempted to fit our event with a two-ribbon flare model as done, for example by Poletto et al. (1988) for the long-duration X-ray flares observed by *Einstein* on Prox Cen and EQ Peg.

2.4. Small amplitude variations

As outlined in Sect. 2, the X-ray light curve of G102-21 shows small-amplitude variations on various time scales. Given the sparse nature of the data it is difficult to assess these variations in detail. Those observed among different time segments could be attributed to rotational modulation making visible (or not) very active regions whose emission is a sizable fraction of the overall stellar coronal emission. Within this scenario, we can analyze the light curve of segment 3 where the emission increases monotonically in the first $\sim$ 2 ksec and thereafter remains constant. If we assume that the observed variation is due to the appearance of an active region at the limb of the star and use the value of rotational velocity obtained from optical observations (see Sect. 3) we can estimate a linear dimension for the active region of 4 10^9cm (rising to 6 10^9cm if we extrapolate the increase of the X-ray emission level to times not covered by our observation). The resulting coverage factor of the stellar surface due to this assumed active region is $\sim 10^{-2}$. If the active region is responsible for the difference between the emission levels in the second half of the segment 3 and during the quiescent phase, its surface flux is $\sim$ 7 10^9erg sec^{-1} cm^{-2}, much higher than that of solar active regions (Peres & Vaiana 1990) and comparable to that typical of solar flares, suggesting that its emission could be due to continuous flare emission.

2.5. EUV data

The ROSAT EUV Wide Field Camera (WFC) is co-aligned with the X-ray telescope / PSPC. During our observation the WFC had the 'S2' filter in place, covering the waveband 112-200 Å. Our source was not detected. In contrast, it *was* detected in the all-sky survey in the S2 waveband at a significance level of 3.5σ, with a rate of 0.014 $\pm$0.005 cnt/sec, while in the S1 band (60-140 Å) there is a 3σ upper limit of 0.010 cnt/sec. The detection in the all-sky survey, where the effective exposure time was about 2000 sec, compared with the longer exposure of the pointed observation, is no surprise due to the large decrease in sensitivity of the WFC following the temporary attitude control failure on 1991 January 25. At the date of the pointed observation, the decrease in photon detection efficiency was a factor $\sim$ 7 for the S1 band and $\sim$ 5 for the S2 band.

Using the empirical correlation of Hodgkin & Pye (1994) between WFC and *Einstein* IPC count rates for late-type stars:

$$1\ [\mathrm{WFC}-\mathrm{S2}]\ \mathrm{count} = 7.2\ [\mathrm{IPC}]\ \mathrm{count}$$

$$1\ [\mathrm{WFC}-\mathrm{S1}]\ \mathrm{count} = 11.1\ [\mathrm{IPC}]\ \mathrm{count} \quad (4)$$

we obtain from the observed WFC-S2 rate, an "equivalent" IPC count rate of 0.1 count/sec, and $\leq$ 0.1 IPC count/sec from the S1 upper limit, both in good agreement with the IPC observation (see above).

We have also compared the WFC and PSPC count rates assuming that during the all-sky survey the star was in a quiescent phase, and have compared the observed EUV emission with that predicted on the basis of the two-temperature spectral modeling of the quiescent X-ray emission seen with the highest statistics in segment 4 of our pointed observation. The rate observed in the S2 filter is comparable with those predicted (0.029 - 0.016) if we assume a value of $\log N_H$ in the range 18.5 - 19, corresponding to the value expected at the star's distance assuming a hydrogen volume density of 0.1 cm^{-3}. The rate predicted in the S1 filter (0.015 - 0.012) is similar to the measured 3 σ upper limit.

3. Optical observations

As discussed in Sect. 1, very limited information is available in the literature, on G102-21. We have therefore started a program of spectroscopic observations to determine the true nature of this active star. We first obtained, thanks to the courtesy of P. Garnavich and D. Crabtree of the Dominion Astrophysical Observatory (DAO) in Victoria, BC, some snapshots of a 600 Å region which includes the Hβ line, at a resolution of about 1.5 Å, and spaced over 4 nights in March 1993. These spectra confirmed the M spectral classification, showing the Hβ line strongly in emission, and with a double peak, suggesting the star to be a binary. Also, the radial velocity appeared to be variable, although, at this resolution and with the double peak of Hβ, it was difficult to assess exactly which component was varying.

To monitor the radial velocity variation in a more systematic way, we tried to obtain further spectra (at DAO). Unfortunately, due to bad weather conditions, only a few spectra could be taken, in the region around Hα, covering 300 Å at about 0.6 Å resolution, which again showed a double peaked structure in the Hα line. The spectra also included the region of the Li I 6708 Å line; it is not detected in absorption. If the Li I line were as strong as it is in dMe pre-main sequence objects (as in the Weak Line T-Tauri stars typically found in the neighborhood of star forming regions, where equivalent widths of a few hundred mÅ for stars as old as a 5 Myr are common, Basri et al. 1991) it would be clearly visible even at this resolution. We can therefore rule out G102-21 as an extremely young object. Lithium is on the other hand burned in the deep convective region of dM stars quite quickly, and therefore the star can still be quite young (ZAMS) and not have a detectable lithium line (D'Antona 1987).

We have further monitored the star at the ESO La Silla 1.5m telescope with the Boller and Chivens spectrograph again us-

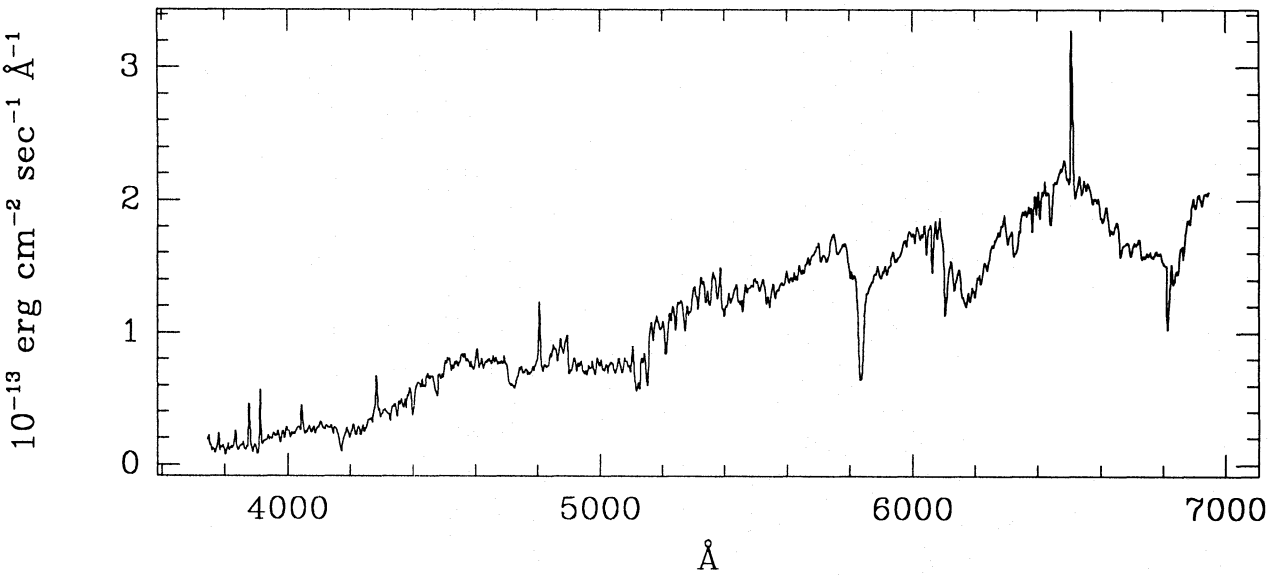

Fig. 6. A low resolution (3.5 Å) spectrum of G102-21, clearly showing the Balmer series and the Ca II H&K doublet in emission

ing some spare time from a program aimed at identifying stellar X-ray sources from *Einstein* observatory surveys. Using the 2048-pixel CCD, the spectral range covered was 3700-7400 Å at approx. 3.5 Å resolution. We observed the star by taking 5 spectra per night for 5 contiguous nights, from January 29, 1994 until February 2, 1994. Using these low-resolution spectra we confirmed the M3 spectral classification and determined a luminosity class V, from the strength of the Na I doublet at 5896-5890 Å, of the MgH band at 4780Å and of the Ca I 4226 Å line. These low resolution spectra show the whole Balmer series, down to Hη, strongly in emission, as well as the Ca II H&K doublet. At this spectral resolution the splitting of the emission lines due to the presence of the two components of the binary system is not visible, although in some of the spectra a widening of the lines is clearly visible. An example of the low resolution spectra is shown in Fig. 6.

We have monitored the equivalent width of the Hα, Hβ and Ca II K lines for the five nights. The equivalent widths clearly vary from night to night, showing an enhancement in night 3 (JD 2449383), where the equivalent width of the Hβ line reached an average value of 4.7 Å, up from an average value of 2.9 Å the night before. The behavior of the three emission lines monitored is, as it can be seen from Fig. 7, rather consistent. The spectrophotometric calibration of the observations is not accurate enough to establish if the absolute flux of the lines also shows similar variations.

We have also taken two spectra of the Hα region at high resolution (about 0.1 Å) at the ESO La Silla 1.4m CAT telescope, again using some spare time from the same stellar X-ray source identification program as at the ESO 1.5m telescope. The spectra were taken on the nights of February 7 and 8, 1994. Both spectra (shown in Fig. 8) show two clearly separated Hα lines in emission, with the separation changing from one night to the other, being 92 km/sec on Feb. 7 and 155 km/sec on

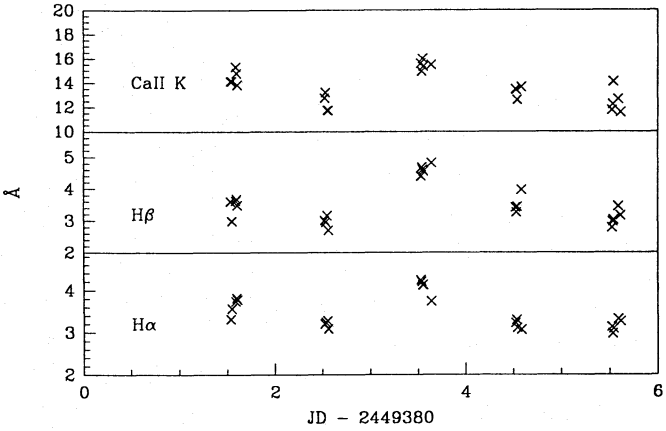

Fig. 7. Time series for the equivalent widths of the Hα, Hβ and Ca II K lines for the 5 nights in which they were monitored

Feb 8. The large change in the radial velocity of the two components indicates that the system is a short-period binary, but the data are obviously not sufficient to determine the orbit. We can, however, put an upper limit on the orbital period by using the largest observed separation. We have assumed a circular orbit and equal mass components. Given the small separation, an orbit with a sizable ellipticity should become circular in a relatively short time; given also that we can rule out extreme youth from the lack of Li I absorption, the assumption of a low eccentricity orbit is a reasonable one. The two spectral systems clearly visible in emission show comparable strengths, as do the two systems of absorption lines visible in the CAT spectra, showing the presence of two components of comparable luminosity and therefore mass. By assuming equal masses and no ellipticity in the orbit we can simplify the classical equation for spectroscopic binaries $V_r = \frac{2\pi a_1 \sin(i)}{P\sqrt{1-e^2}}(e\cos(\omega) + u)$ (Lang

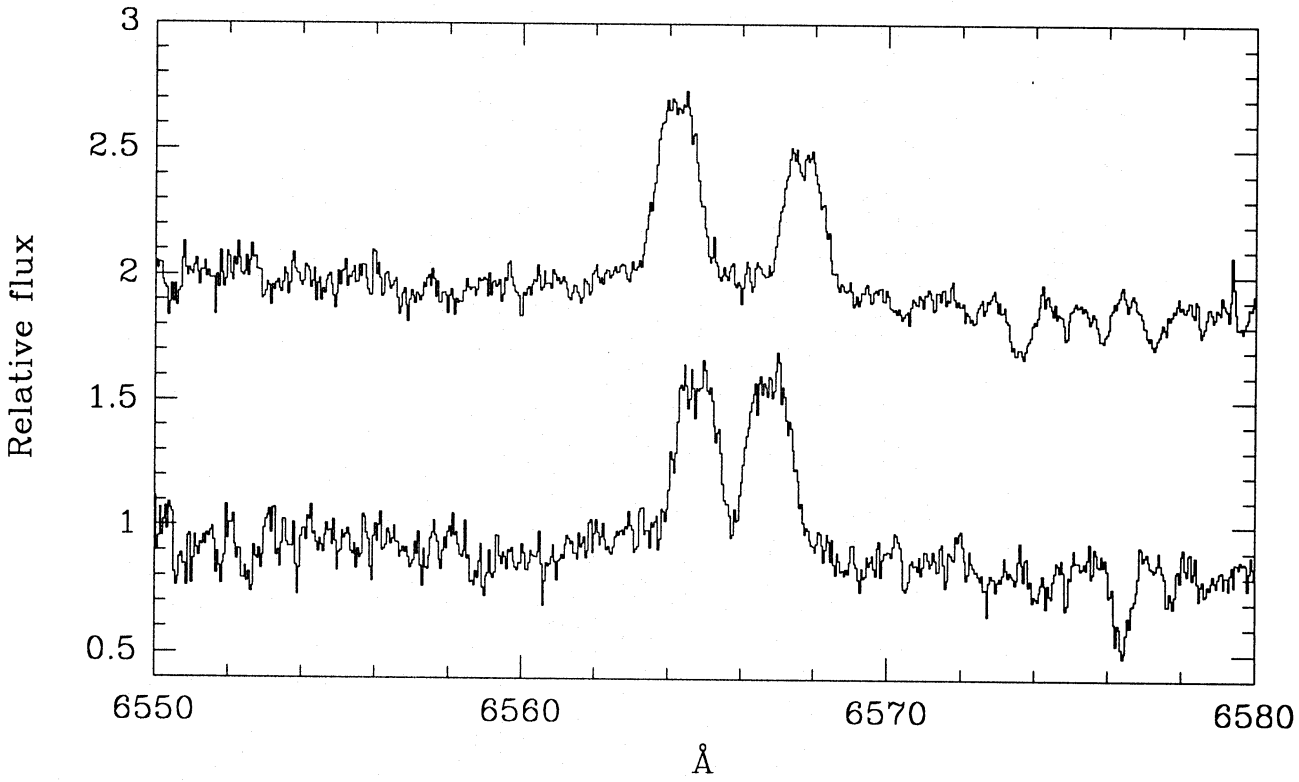

Fig. 8. High resolution spectra of the Hα region for G102-21, taken at the ESO CAT on February 6 (bottom) and 7 (top) 1994

1980) into $V_r = \frac{\pi a \sin(i)}{P} \cos(\omega)$, or $\Delta V_r = \frac{2\pi a \sin(i)}{P}$, where ΔV_r is the difference between the maximum and minimum radial velocities (in our case 155 km/s). By using Kepler's third law in the form $a^3 = GP^2(M_1 + M_2)/(4\pi^2)$, assuming $M_1 = M_2$ and substituting we get the relationship

$$P = \frac{4\pi GM}{(\Delta V_r)^3} \sin^3(i). \quad (5)$$

By assuming $M = 0.3 M_{Sun}$ (appropriate for a dM3 star) we get $P \lesssim 1.55 \sin^3(i)$ *days* (we quote P as an upper limit to the true value of the period because the observed ΔV_r is only a lower limit to the true maximum ΔV_r).

By also assuming a tidally locked binary, i.e. with the rotational period equal to the orbital period we have just derived, and the stellar radius appropriate for a dM3 star (0.4 solar radii, or $2.77 \cdot 10^{10}$ cm) we obtain a surface rotational velocity $v \geq 13/\sin^3(i)$ km/sec. We can also measure the rotational broadening of the photospheric absorption lines visible in the CAT spectra, using the calibration for the CAT of Favata et al. (1994), obtaining a value for the surface rotational velocity of $v \cdot \sin(i) = 20$ km/sec, with a formal error of 2 km/sec, compatible with the value derived from the tidal locking hypothesis. By assuming complete tidal locking, we can impose the condition that $13/\sin^3(i) = 20/\sin(i)$ and from this derive a value for the orbital inclination, obtaining $i \sim 50°$, which would give a period $P \lesssim 0.72$ *days*.

We have also used the high resolution spectra of the Hα line taken both at DAO and at the ESO CAT to compute the radial velocity of the barycentre of the system (computed as the average of the radial velocity of the two Hα emission components) finding it to be about 130 km/sec. By using the published proper motion values and the method of Johnson & Soderblom (1987), we can compute the space velocities relative to the Sun, finding [U, V, W] = [-120, -47, -29]. These space-velocity components are high and therefore indicative of a kinematically old system. According to the method of Eggen (1973a, 1973b, 1973c), who has established regions in the U, V plane, based on observational evidence from nearby B, A, F and G stars, G102-21 falls well away from the region typically occupied by young disk stars, and at the edge of the elliptical region occupied by the old disk population, close to the region typically occupied by halo population stars. On the criterion of Upgren (1978), which uses the absolute value of the W velocity component (the component perpendicular to the Galactic disk), separating young and old disk stars on the basis of $|W|$ respectively being smaller and greater than 15 km/s, G102-21 appears to be an old object. Finally, the method utilising peculiar velocity ($V_{pec} = \sqrt{(U^2 + V^2 + W^2)}$, Meusinger et al. 1991), which discriminates young and old disk objects on the basis of V_{pec} respectively being greater and smaller than 40 km/s, indicates G102-21 as a likely old object. Kinematic criteria alone, given their statistical nature, are clearly not sufficient to establish the age of a single object, however the high space velocities of G102-21 are typical of a (very) old object and not compatible with its being a young object.

To summarize, the optical observations show that G102-21 is a short period binary with two dM3 components, with a relatively high (for its spectral type) surface rotation, which leads to a high level of stellar activity, as evident in both the X-ray emission and the emission lines in the optical spectrum. The space velocity of G102-21 makes it a kinematically old object, with values marginally compatible with being a halo object. Therefore its high level of activity (typical of young stars) does not agree with the kinematically determined age. Rather, the enhanced activity would, in this case, be the result of the high rotational velocity due to the tidal locking between orbital and rotational period. Further studies of G102-21 will surely help clarify the nature of this interesting object. In particular, a trigonometric parallax determination would be useful. Also, we expect G102-21 to exhibit a high frequency of flaring, and therefore monitoring at all wavelengths, including optical photometry, would additionally be useful to detect (possible) optical eclipses. In this respect, note that a recent campaign of photometric measurements (Pagano et al. 1994) has shown the occurrence of very large ($\Delta\ U\ > 7$ mag) optical flares on G102-21. We are planning to monitor the radial velocity to obtain the orbital elements in a forthcoming observational campaign.

4. Summary and conclusions

We have presented the X-ray detection of the very active nearby dMe star G102-21. The quiescent emission of the star in the ROSAT band (0.2-2.4 keV) is $\sim 7\ 10^{28} erg/sec$, typical of the most intense young M stars in the solar neighborhood. The star's X-ray emission shows variations of various amplitudes on several time scales. The most intense variation has been interpreted as the occurrence of a "compact" flare with physical parameters similar to those observed in other dMe stars, with EXOSAT. Other, lower amplitude variations have been interpreted as due to a combination of rotational modulation and emergence of active regions on the visible part of the stellar surface.

Spectroscopic observations have allowed us to detect emission in the whole Balmer series and in the CaII H&K lines. High resolution observations have shown the presence of two companions of similar spectral type and with similar activity level.

Combining X-ray and spectroscopic measurements, with simple assumptions, we are able to verify the consistency of the data with our suggestion that small X-ray variations are mainly due to rotational modulation. First of all we assume that all the small variations we observe in X-rays are due to a single very bright active region on the stellar surface of one of the companions and ignore possible effects due to differential rotation and active region longitudinal migration. In this approximation, when the active region is on the visible side of the stellar surface we observe an enhancement of X-ray emission (time segments 3, 5, 7, and 8). In the quiescent phases (time segments 1, 2, 4, and 6) the active region is on the night side, and finally, and the active region is just arriving on the day side at segment 3. We assume also that the flare we observe in segment 5 is associated with the same active region. We note that the linear dimensions

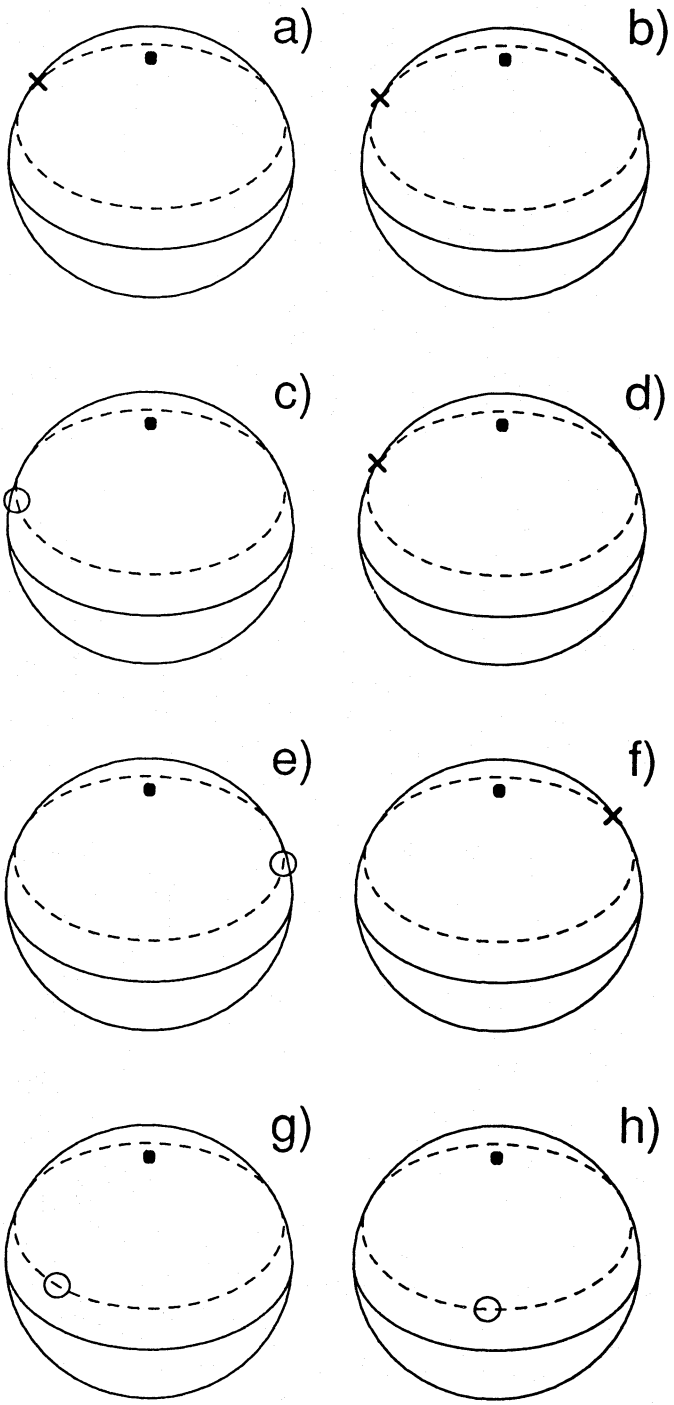

Fig. 9. Position of the stellar active region responsible for the enhancement of the X-ray emission during the ROSAT observation. The solid point indicates the pole position. The little open circle indicates the position of the active region when it is on the visible side of the star, the cross indicates its position when it is on the other side. If we let $\phi = 0$ in the first segment of the observation (panel a), we obtain $\phi = 0.03$ for second segment (panel b), $\phi = 0.11$ for segment 3 (panel c), $\phi = 2.03$ for segment 4 (panel d), $\phi = 2.58$ for segment 5 (panel e), $\phi = 2.68$ for segment 6 (panel f), $\phi = 5.22$ for segment 7 (panel g), $\phi = 5.33$ for segment 8 (panel h)

as deduced for the active region in segment 3 (see Sect. 2.4) are consistent with those obtained from the analysis of the flare, hence this assumption is compatible with the data.

By requiring that the active region be visible in segments 3, 5, 7, and 8 and not in the other segments, we constrain the period to lie between 14 and 15 hours, irrespective of the inclination of the stellar rotation axis.

Assuming a period of 15 hours and substituting it in eq. 5 we obtain a value of $i \sim 50°$ in agreement with the value derived from the rotational broadening measurements. Figure 9 illustrates the position of the active region on the stellar surface in each of the eight time segments we have considered. We note that the first 3 segments of observations are taken within a small fraction of the putative period, segments 4, 5, and 6 fall in the third period, and segments 7 and 8 fall in the sixth period.

The results we have presented for this very active dM star demonstrate (even though based on very simple assumptions) the feasibility of monitoring very active nearby late-type stars to search for rotational modulation in X-rays, and show the ability of X-ray surveys to find otherwise neglected very active late-type stars in the solar neighborhood.

Acknowledgements. G.M. and S.S. acknowledge financial support from ASI (Italian Space Agency), and MURST (Ministero della Università e della Ricerca Scientifica e Tecnologica). J.P. acknowledges the financial support of the UK Particle Physics and Astronomy Research Council. We thank A. Maggio, F. Reale, S. Serio and the referee P. B. Byrne for their helpful comments. During this work we have extensively used the Simbad database.

References

Ambruster, C., Sciortino, S. & Golub, L. 1987, ApJS, 65, 273.
Avni, Y. 1976, ApJ, 210, 642
Barbera, M., Micela, G., Sciortino, S., Harnden, F. R., Jr. & Rosner, R. 1993, ApJ, 414, 846.
Basri, G., Martin, E.L., Bertout, C. 1991, A&A, 252, 625
D'Antona, F. 1987, ApJ, 320, 653
Eggen, O.J. 1973a, PASP 85, 289
Eggen, O.J. 1973b, PASP 85, 379
Eggen, O.J. 1973c, PASP 85, 542
Favata, F., Rosner, R., Sciortino, S., Vaiana, G.S. 1988, ApJ, 324, 1010
Favata, F., Barbera, M., Micela, G. and Sciortino, S. 1994, A&A, in press.
Fiore, F. , Elvis, M., Siemiginowska, A., Wilkes, B., & McDowell, J. C. 1994, ApJ, submitted.
Fleming, T. A., Gioia, I. & Maccacaro T. 1989, AJ, 98, 692.
Giacconi, R. et al. 1979, ApJ, 230, 540
Giampapa, M. S., Golub, L., Peres, G., Serio, S., Vaiana, G. S. 1985, ApJ, 289, 203.
Giclhas, H. L., Burnham R. and Thomas N.G. 1963, Lowell Obs. Bull, 6, 1.
Gliese, W., Jahreiss, H. 1991, Third Catalog of Nearby Stars (CSN3), Veröffentl. Astron. Rechen-Institut, Heidelberg, in preparation, (as supplied on NSSDC CD-ROM).
Harnden, F. R., Jr., Sciortino, S., Maggio, A., Micela, G., Vaiana, G. S., Schmitt, J., and Rosner, R. 1990, in Imaging X-ray Astronomy, M. Elvis, ed., Cambridge University Press, 313
Hodgkin, S. T., and Pye, J. P., 1994, MNRAS, 267, 840
Jeffries, R. D., and Bromage, G. E. 1993, MNRAS, 260, 132
Johnson, D.R.H. and Soderblom, D.R. 1987, AJ 93, 864
Lang, K.R. 1980, Astrophysical Formulae, Springer-Verlag, Berlin
Lee, S.-G. 1984, AJ, 89, 702
Landini, M., Monsignori-Fossi, B. C., Paresce, F. & Stern, R. A. 1985, ApJ, 289, 709.
Lemen, J. R., Mewe, R., Schrijver, C. J. & Fludra, A. 1989, ApJ, 341, 474.
Maggio, A., Sciortino, S., & Harnden, F. R., Jr. 1994a, Proceeding of the ROSAT Science Symposium, eds. E. Schlegel and R. Petre, American Institute of Physics, 244
Maggio, A., Sciortino, S., & Harnden, F. R., Jr. 1994b, ApJ, 432, 701
Meusinger, H., Reimann, H.G. and Stecklum, B. 1991, A&A 245, 57
Ottmann, R. 1993, A&A 273, 546.
Ottmann, R., Schmitt, J.H.M.M., Kurster, M. 1993, ApJ, 413, 710.
Pagano, I, Ventura, R., Rodonò, M., Peres, G. & Micela, G. 1994, submitted, A&A
Pallavicini, R., Serio, S. & Vaiana, G. S. 1977, ApJ, 216, 108.
Pallavicini, R., Tagliaferri, G. & Stella, L. 1990, A&A, 282, 403.
Pallavicini, R. 1993, in "Advances in Solar and Stellar Coronal Physics", J. Linsky and S. Serio (eds.), Kluwer Publishing Company, 237.
Peres, G., & Vaiana, G.S. 1990, MemSAIt, 61, 401
Pfeffermann E., et al. 1986, Proc. SPIE, 733, 519
Poletto, G., Pallavicini, R., Kopp, R. A. 1988, A&A, 201, 93
Pounds, K. A., et al., 1993, MNRAS, 260, 77
Raymond, J., & Smith, B. W. 1977, ApJS, 35, 419
Raymond, J. 1988, in Hot and Thin Plasmas in Astrophysics, ed. R. Pallavicini, Kluwer Academic Publisher, 3
Reale, F., Peres, G., Serio, S., Rosner, R., & Schmitt, J.H.M.M. 1988, ApJ, 328, 256.
Reale, F., Serio, S., & Peres, G. 1993, A&A, 272, 486.
Reichert, G. A. 1993, The ROSAT IDL Recipes cookbook (Greenbelt, MD: Goddard Space Flight Center)
Serio, S., Reale, F., Jakimiec, J., Sylwester, B., & Sylwester, J. 1991, A&A, 241, 197.
Schmitt, J.H.H.M, Harnden, F. R. Jr., Rosner, R., Peres, G., Serio, S. 1985, ApJ, 288, 751.
Schrijver, C. J., Lemen, J. R., Mewe, R. 1989, ApJ, 341, 484.
Sciortino, S., Favata, F., & Micela, G., 1995, A&A in press.
Sciortino S., Harnden, F. R., Jr., Maggio, A., Micela, G., Vaiana, G. S., Schmitt, J., and Rosner, R. 1988, in Astronomy from Large Database, ESO Conference and Workshop Proceedings No. 28, 483
Sims, M.R., et al. 1990, Opt. Eng., 29, 649
Smale, A.P., Charles, P.A., Corbet, R.H.D., Jordan, C., Brown, A., & Walter, F. 1986, MNRAS, 221, 77.
Snowden, S. L., McCammon, D., Burrows, D. N., & Mendenhall, J. A. 1994, ApJ, 424, 714.
Stern, R. A., Antiochos, S. K., Harnden, F. R. Jr. 1986, ApJ, 305, 417.
Upgren, A.R. 1978, ApJ 83, 626
Vaiana, G.S., & Rosner, R. 1978, ARA&A, 16, 393
Vaiana, G.S., et al. 1981, ApJ, 245, 163.
Zimmermann, H. U., Belloni, T., Izzo, C., Kahabka, P., Schwentker, O. 1993, EXSAS User's Guide Third Edition, MPE Report 244, ISSN 0178-0719.
White, N. E., & Peacock, A. 1988, MemSAIt, 59, 7

This article was processed by the author using Springer-Verlag LaTeX A&A style file version 3.